Superconductor
Science and
Technology

PURPOSE-LED
PUBLISHING™

PAPER • **OPEN ACCESS**

Effects of the pseudo-gap on the superconducting performance of $Bi_2Sr_2CaCu_2O_x$ round wires

To cite this article: Chiara Tarantini *et al* 2026 *Supercond. Sci. Technol.* **39** 085006

View the article online for updates and enhancements.

You may also like

- Understanding processing–microstructure–properties relationships in $Bi_2Sr_2CaCu_2O_x$/Ag round wires and enhanced transport through saw-tooth processing
Golsa Naderi, Xiaotao Liu, William Nachtrab et al.

- Variation of effective filament diameter, irreversibility field, anisotropy, and pinning efficiency in Bi-2212 round wires
Chiara Tarantini, Shaon Barua, Temidayo Abiola Oloye et al.

- The behavior of grain boundaries in the Fe-based superconductors
J H Durrell, C-B Eom, A Gurevich et al.

This content was downloaded from IP address 146.201.200.116 on 02/11/2026 at 18:24

Superconductor Science and Technology

Check for updates

OPEN ACCESS

RECEIVED
27 March 2026

REVISED
19 June 2026

ACCEPTED FOR PUBLICATION
27 July 2026

PUBLISHED
6 August 2026

Original content from this work may be used under the terms of the Creative Commons Attribution 4.0 licence.

Any further distribution of this work must maintain attribution to the author(s) and the title of the work, journal citation and DOI.

PAPER

Effects of the pseudo-gap on the superconducting performance of $Bi_2Sr_2CaCu_2O_x$ round wires

Chiara Tarantini[1,*], Shaon Barua[1], Jianyi Jiang[1], Fumitake Kametani[1,2], Eric E Hellstrom[1,2] and David C Larbalestier[1,2]

[1] Applied Superconductivity Center, National High Magnetic Field Laboratory, Florida State University, Tallahassee, FL 32310, United States of America

[2] Department of Mechanical & Aerospace Engineering, FAMU-FSU College of Engineering, Florida State University, Tallahassee, FL 32310, United States of America

[*] Author to whom any correspondence should be addressed.

E-mail: tarantini@asc.magnet.fsu.edu

Keywords: superconductivity, pseudo-gap, $Bi_2Sr_2CaCu_2O_x$, irreversibility field, critical current density

Supplementary material for this article is available online

Abstract

$Bi_2Sr_2CaCu_2O_x$ (Bi-2212) is an interesting high temperature superconductor (HTS) for high field applications due to its unique ability to develop high critical current density (J_c) in polycrystalline round wires. The performance of all HTSs is highly sensitive to the doping states, particularly near the critical doping where the pseudo-gap opens and J_c, the upper critical field H_{c2} and other superconducting properties, but not T_c, are maximized. However, due to Bi-2212's complex wire microstructure, the impact of doping on the conductor performance has been poorly understood. Here we systematically investigate the superconducting behaviour across a wide doping range, separating for the first time the individual effects induced by oxygen-doping on the grain and the grain boundary (GB) properties. Our results can be interpreted as grains and GBs being affected by separate pseudo-gap openings with the grain irreversibility field H_{Irr} being controlled solely by the grain pseudo-gap, whereas the GB H_{Irr} is influenced by both. Moreover, the J_c performance at 4.2 K is strongly related to the grain vortex pinning properties, but with some J_c limitation arising from the GBs. These findings demonstrate the impact of a fundamental physical phenomenon, the pseudo-gap, on the overall conductor performance, and they highlight the complexity of optimizing this material. These results also suggest that targeted adjustments to Bi-2212 processing may enable significant improvements in J_c. Moreover, since the pseudo-gap is not unique to Bi-2212, similar limiting effects of different grain and GB boundary doping almost certainly operate in other HTSs, which also could gain from alternative processing strategies making them more suitable for magnets for high-field research, fusion or medical applications, and for high-power cable technologies.

1. Introduction

$Bi_2Sr_2CaCu_2O_x$ (Bi-2212) is a particularly interesting material from both the physical and technological perspectives and because of their interactions. From the physical standpoint, all cuprate high temperature superconductor (HTS) are unconventional and cannot be explained by the BCS theory [1]. They exhibit *d*-wave pairing symmetry, resulting in nodal superconducting order parameter, a feature many think limits supercurrent flow across high-angle grain boundaries (HAGB). Moreover, cuprates possess very complex phase diagrams encompassing a variety of physical phenomena like poor or strange metal behaviours, antiferromagnetism at low doping level, spin/charge/superconducting fluctuations, pseudo-gap, charge and spin density waves, Fermi liquid and superconductivity [2].

Keys to this study on Bi-2212 wires are the superconducting dome in the hole-doped state and the pseudo-gap regime. Presland *et al* [3] described the doping-dependence of the dome with a universal

© 2026 The Author(s). Published by IOP Publishing Ltd

parabolic relation for all cuprates, $T_c = T_{c,max}\left[1 - 82.6(p-0.16)^2\right]$, with T_c and p being the critical temperature and number of holes per Cu. Since the actual doping level is hard to directly evaluate, this formula has been widely used to evaluate p from measured T_c allowing also an easy comparison with previous works. The optimal doping for the maximum of T_c ($T_{c,max}$) is at $p_{opt} = 0.16$ hole/Cu (in the following we will omit hole/Cu). Doping below p_{opt} is referred as under-doped and above as over-doped.

There is an exceptionally vast literature on the various physical phenomena occurring in cuprates both above and below T_c, and here we summarize the different hypotheses about the pseudo-gap phase boundary. In hole-doped Bi-2212, the doping level at which the pseudo-gap closes with increasing p is controversial for both its position and temperature dependence. Such closure was located at a 'critical doping' p_c of ~0.19 by thermodynamic and ARPES measurements down to low temperatures within the superconducting dome [4–6]. However, other scenarios were suggested (e.g. by STS, Raman, NMR, ARPES, transport,…) with the pseudo-gap persisting up to very high temperature above T_c and being limited by a $T^*(p)$ line in the phase diagram (see for instance [7, 8] for overviews). Some studies suggested that the high-temperature $T^*(p)$ line meets the superconducting dome at $T_{c,max}$, whereas others reported shifts to higher over-doping level. Also different $T^*(p)$ trends were suggested within the dome, considering 'entrant' or 'reentrant' behaviours (i.e. $T^*(p)$ with negative or positive slope below T_c joining the point where $T^*(p)$ above T_c meets the dome, with p_c ~0.19 at 0 K), as well as no pseudo-gap below or a complete temperature independent closure of the pseudo-gap at p_c [6, 7, 9]. Despite these differences, most scenarios agree with a critical doping of $p_c \sim 0.19$ at low temperature. The reason for considering this fundamental physical phenomenon in the study of wires is that the pseudo-gap amplitude increases linearly with decreasing p below p_c and its opening appears to compete with superconductivity (due to reduction in density of states) leading to maxima at p_c of the condensation energy, J_c, and H_{c2} (maximum H_{c2} at $p_c \sim 0.183$ in Bi-2212) [4, 10, 11], thereby affecting the wire performance.

From the technological perspective, Bi-2212 is unique among HTS conductors for its ability to be made into a superconducting round wire, ideal for high-field, low-temperature applications [12]. In general, the primary obstacle of making HTS round wire lies in the material high anisotropy and the detrimental effects of grain-to-grain misorientation. In other HTS this issue is overcome by two approaches: creating a highly complex multilayer tape, which induces long-length bi-axial texture in the epitaxial superconducting film, as in $REBa_2Cu_3O_x$ (or REBCO, with RE = rare earth) tapes; producing powder-in-tube (PIT) multifilamentary tapes, such as $Bi_2Sr_2Ca_2Cu_3O_x$ (Bi-2223), whose partial texture is induced by mechanical flat rolling. The disadvantages of both tapes are the large aspect ratio of their cross-sections as well as their strongly anisotropic performance, both undesirable features for most high-field applications. Moreover, REBCO is effectively a single-filament conductor, so vulnerable to local defects or damage and preventing current sharing, and has a wide tape superconducting cross-section, undesirable because of the large, induced screening current. Bi-2223 is polycrystalline with only a uniaxial c-axis texture perpendicular to the tape and no in-plane texture, so its performance suffers from in-plane HAGB. The peculiarity of Bi-2212 is that it can be made in polycrystalline round wire via PIT method (see cross sections in figures 1(c) and (d)), it has the advantage that during the over-pressure heat treatment (OPHT) it melts and the slow cooling promotes grain nucleation with a rapid a-axis growth, enabling grain self-alignment. This leads to a unique local bi-axial texture with the c-axis of the polycrystals rotating along the filaments [13]. Consequently, Bi-2212 multifilamentary wires exhibit macroscopically isotropic properties and excellent current transfer capability, highly desirable for magnet applications.

In this study, we explore the effects of de-oxygenation and over-oxygenation on Bi-2212 round wire, examining the resulting superconducting performance and its correlation with more fundamental aspects. In particular, we address several open questions. Although the typical OPHT sets Bi-2212 in a slightly over-doped state that maximizes J_c, what is the actual p concentration? Is there a significant difference between the grain and the GB doping states? How and how much are the doping states affecting the various superconducting properties? Is there a way to improve the superconducting performance of the wire?

2. Method

2.1. Sample preparation

The Bi-2212 conductor employed for this work consists of 990 filaments organized into 18 bundles with 55 filaments each (55 × 18 restack design, figure 1(c)). The Bi-2212 filaments are embedded in an Ag matrix forming a 1 mm-diameter wire with an average filament diameter of 14.4 μm (wire ID:

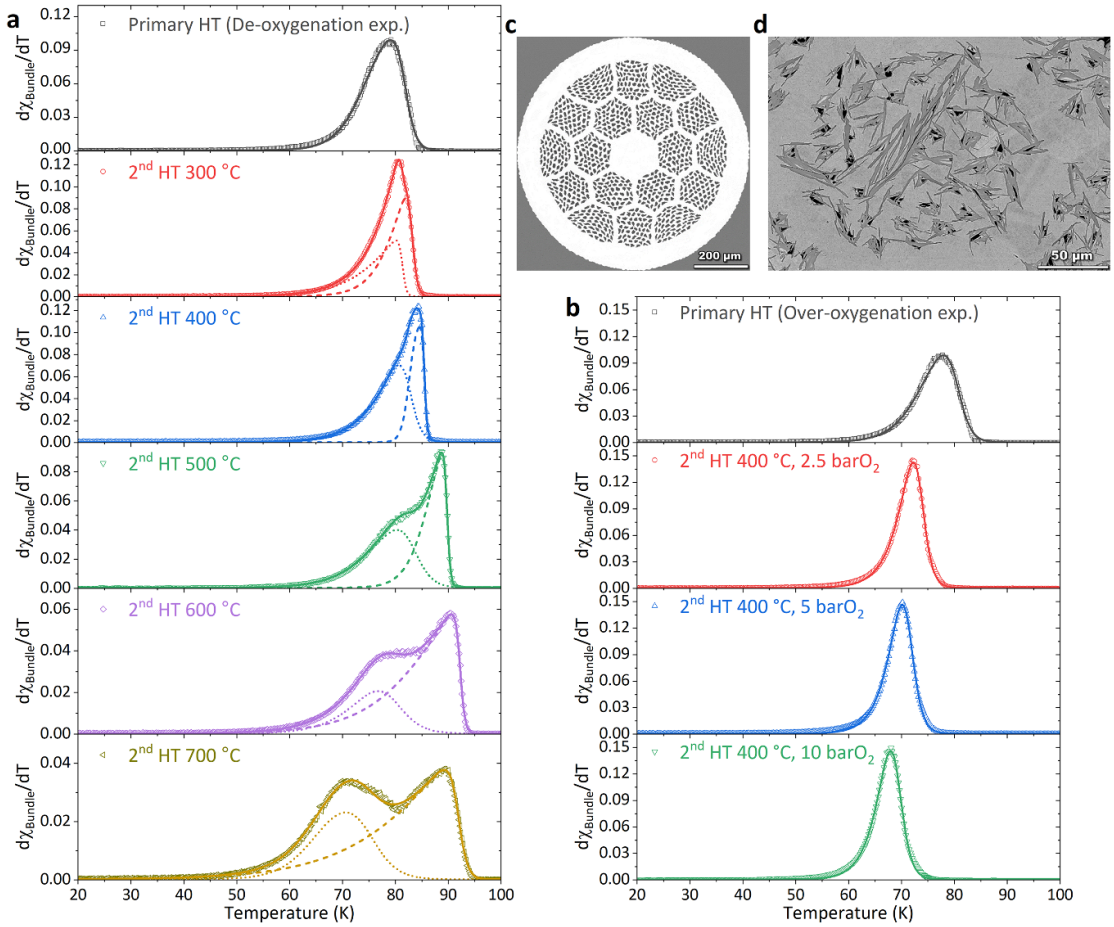


Figure 1. (a) Derivatives of the magnetization superconducting transitions of $Bi_2Sr_2CaCu_2O_x$ samples measured by DC susceptibility after a zero-field-cooling performed on primary and de-oxygenated sample and (b) on primary and over-oxygenated samples (see table 1). The dashed, dotted and solid lines are the results of the single or double-peak fitting. Panel (a) demonstrates the separation, upon de-oxygenation, of the grain and grain boundary superconducting transitions (higher and lower temperature peaks, respectively) and their non-monotonic shifts. Panel (b) reveals that, upon over-oxygenation, the transitions become sharper and progressively move towards lower temperatures. (c) Transverse cross section of the entire wire after the pre-densification heat treatment (before the overpressure heat treatment reaction). (d) Backscattered-electron scanning electron microscope image of a typical $Bi_2Sr_2CaCu_2O_x$ bundle after the over-pressure heat treatment. Panels (c) and (d) show the typical conductor microstructures before and after the over-pressure heat treatment. In the first case the filaments are discrete and organized in 18 bundles with 55 filaments each. After reaction the filaments within each bundle tend to bond.

pmm180627). After a 50 bar pre-densification HT at 830 °C/12 h, segments of the wire underwent a primary OPHT, as described in [14], reaching a maximum temperature of ∼889 °C (actually 888.5 °C for the de-oxygenated and 889.5 °C for the over-oxygenated samples; the small differences in the primary heat-treated samples is due to the small HT difference and the high sensitivity of Bi-2212 to subtle processing changes). The primary HT typically results in limited filament bonding within the bundles (figure 1(d)). Following the primary OPHT, the Bi-2212 samples underwent secondary HTs to modify their oxygen content. De-oxygenation was accomplished by heating the samples at temperatures ranging between 300 and 700 °C in a partial O_2 pressure of 0.01 bar for 48 h. Over-oxygenation was performed by heat treating at 400 °C in a O_2 pressures of 2.5, 5 and 10 bar for 48 h. Table 1 summarized the conditions and sample names corresponding to these secondary treatments.

2.2. Superconducting and microscopic characterizations

Magnetic characterizations were performed on ∼4 mm long samples with the magnetic field applied perpendicularly to the wire axis. DC magnetization measurements for all samples were carried out in a Quantum Design (QD) MPMS SQUID magnetometer at 1 mT to determine the superconducting transition and to evaluate the average bundle size as explained in [15, 16]. From these measurements, the DC susceptibility evaluated over the bundle volume, χ_{Bundle}, was obtained (see supplementary figure S1) along with its derivative $d\chi_{Bundle}/dT$ (figure 1). Peak positions of $d\chi_{Bundle}/dT$ were determined using single asymmetric peak fits for the primary and over-oxygenated samples, and double asymmetric peak fits for de-oxygenated samples. The resulting peak modes were taken as the corresponding T_c values.

Table 1. Summary of the secondary heat treatment (2nd HT) conditions performed on the $Bi_2Sr_2CaCu_2O_x$ wire after the primary over-pressure heat treatment. Those secondary heat treatment changed the doping state of $Bi_2Sr_2CaCu_2O_x$.

Preparation	Name	2nd HT temperature	2nd HT pressure
	Primary	—	—
De-oxygenation experiment	300 °C	300 °C	
	400 °C	400 °C	$P_{tot} = 1$ bar
	500 °C	500 °C	$P_{O2} = 0.01$ bar
	600 °C	600 °C	$P_{Ar} = 0.99$ bar
	700 °C	700 °C	
	Prim.2	—	—
Over-oxygenation experiment	2.5 $barO_2$	400 °C	$P_{tot} = P_{O2} = 2.5$ bar
	5 $barO_2$		$P_{tot} = P_{O2} = 5$ bar
	10 $barO_2$		$P_{tot} = P_{O2} = 10$ bar

Considerations regarding the choice of the fitting function are given in the supplementary materials and in figures S2 and S3.

AC susceptibility was measured in a QD 9 T PPMS with $\mu_0 H_{DC}$ up to 9 T and $\mu_0 H_{ac}$ ranging from 0.1 to 1.5 mT ($f = 73$ Hz, chosen to limit the current induced into the Ag matrix), as we previously demonstrated that this technique allows us to separately investigate the intra and INTER-grain contributions by analysing the first harmonic χ_1'' dissipation peak (also the AC susceptibility is evaluated on the bundle volume). Since the irreversibility line (IL) is by definition at $J_c = 0$, where the vortex pinning energy also vanishes, and J_c is proportional to H_{ac} [17], investigating the shift of the dissipation peaks as H_{ac} approaches zero enables determination of the intra and INTER-grain ILs, as described in [15, 16].

The critical current of the wires was measured in transport using the four-probe method and estimating I_c at the typical electric field criterion of 1 μV cm^{-1}. Measurements were carried out at 4.2 K in magnetic field of 5 T applied perpendicular to the wire axis. Corresponding J_c values were determined by dividing I_c by the densified cross-sectional area of the filaments after the 830 °C/12 h pre-densification process [18].

The Bi-2212 cross-sectional area after powder densification was evaluated by analysing optical images acquired with an Olympus BX1M-LED optical microscope. Backscattered electron imaging was performed in a FEI Helios G4 UC dual beam (electron and Ga ion) field emission scanning electron microscope on polished transversal cross-sections of the wires after the OPHT.

3. Results

3.1. Tuning the doping states

The superconducting transitions were first evaluated by DC susceptibility (supplementary figure S1). To highlight the features of the transitions, the temperature derivative of the susceptibility curves was analysed as shown in figures 1(a) and (b). In a homogeneous, well-connected superconductor $d\chi/dT$ typically exhibits a single peak in correspondence of the transition with minor broadening on the low-temperature side. Here, after the primary HT, the peak was slightly broadened, suggesting the presence of two partially overlapping peaks. Upon initial de-oxygenations of Bi-2212 up to 400 °C, the transition temperature increased and the separation of the two partially overlapping $d\chi_{Bundle}/dT$ peaks became more obvious (figure 1(a)). Further de-oxygenation at 500 °C–600 °C caused the higher-temperature peak to shift upward, while the lower-temperature peak moved downward. Only after the de-oxygenation at 700 °C did both peaks shift toward lower temperatures.

In the over-oxygenation experiment performed at increasing O_2 pressure (figure 1(b)), single peaks, much sharper than after the primary HT, are observed with position progressively shifting to lower temperatures. To estimate the positions of those peaks, we performed single and double peak fits (see section 2.2). The double transitions observed in the de-oxygenated samples, are typically attributed to separate grain contribution (or intra-grain) for the higher-temperature feature and to GB contribution (or inter-grain) for the lower-temperature feature.

To evaluate the doping state p of both the grains and the GBs, we employed the positions of the peak maxima from the fits in figure 1 as T_c values and applied Presland's parabolic relation for $T_c(p)$ [3]. Assuming the maximum T_c values observed in the de-oxygenated series for the grains and the GBs as $T_{c,max}$ in Presland's relation, we built the diagram in figure 2 (possible effects on p on the choice of

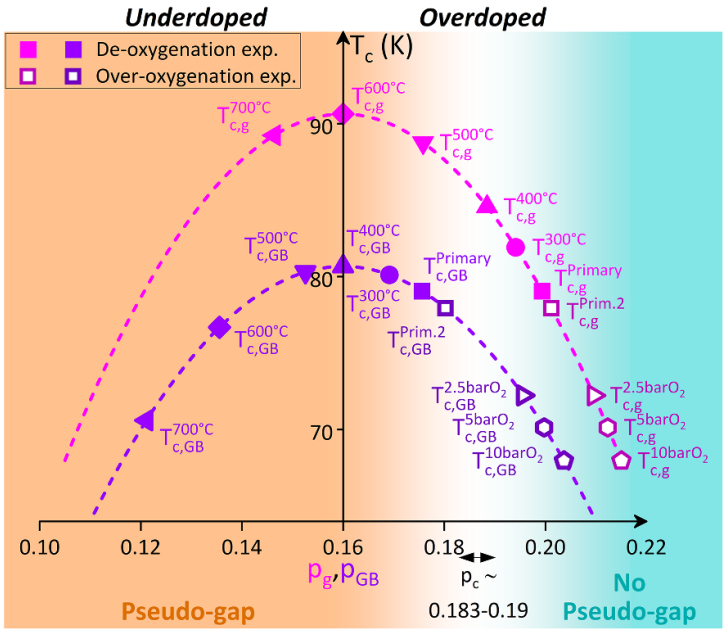


Figure 2. Diagram of critical temperature T_c as a function of the doping level p for the grain and grain boundaries obtained on $Bi_2Sr_2CaCu_2O_x$ samples. The grain and grain boundaries critical temperatures $T_{c,g}$ and $T_{c,GB}$ were determined from figure 1. The full and open symbols are for the de-oxygenated and over-oxygenated series, respectively. Identical symbol shapes on the two main curves are for the same sample. The correspondent doping levels p_g and p_{GB} were calculated by using Presland's parabolic relation. The under-doped ($p_g, p_{GB} < 0.16$) and over-doped ($p_g, p_{GB} > 0.16$) states are determined with respect to the maximum position. The critical doping p_c, below which the pseudo-gap is expected to open, is assumed to be at about 0.183–0.19. The data point labels have subscripts 'g' or 'GB' for grain or grain boundaries, and superscripts reporting the name/heat-treatment conditions as described in table 1. This diagram evidences the markedly different T_c values of the grain and grain boundary with changing the doping states making them independently affected by the presence or absence of the pseudo-gap.

the $T_{c,max}$ values are described in the supplementary materials). This generates two curves, one for the grain properties (marked by the subscript 'g') and one for the GB properties (marked by 'GB'). Note that, having fitted the data for the primary-heat-treated and the over-oxygenated samples with a single peak function, the two T_c values are assumed identical. It must be kept in mind, however, that in the over-oxygenated samples we cannot exclude that the local GB $T_{c,GB}$ of being higher than $T_{c,g}$ (a locally higher $T_{c,GB}$ would be undetectable by magnetization), so for these three samples $T_{c,GB}$ could be underestimated. A higher $T_{c,GB}$ with a corresponding lower p_{GB} for the over-oxygenated samples could occur in case of similar or only slightly different grain and GB diffusion rates, due to the large difference in the initial p concentrations observed in the primary heat-treated sample. The p_g and/or p_{GB} concentrations estimated in figure 2 are used in the following as parameter of other superconducting properties with respect to the doping levels. The $T_c(p)$ trends clearly shows that $T_{c,GB}$ maximum is reached by deoxygenating at 400 °C, whereas $T_{c,g}$ maximum is obtained only at 600 °C, implying that the GBs are more rapidly affected by de-oxygenation. The two $T_c(p)$ curves also evidence a marked difference in the grain and GB $T_{c,max}$ values, possibly caused by variations in the microstructure, microchemistry and strain at the GBs.

Looking closely at the T_c doping dependences in figure 2, according to the previously identified threshold p_c for the opening of the pseudo-gap, we noticed that the primary-heat-treated samples have their GBs within the pseudo-gap regime ($p_{GB} < p_c$), whereas the grains are at a doping level without pseudo-gap ($p_g > p_c$). Moreover, over-oxygenation brings both the grains and the GBs into the non-pseudo-gap region.

3.2. Variation of irreversible properties with the doping state

AC susceptibility measurements are a valuable tool to investigate the properties of Bi-2212 wires [15, 16]. Analysing the dissipative part χ_1'', we can distinguish the contributions determined by long-range induced current, which must cross the GBs (referred in the following by GBs), and by short-range currents confined within the grains (see supplementary figure S4). The corresponding ILs for both the grains and the GBs are shown in figure 3. Upon de-oxygenation (figures 3(a) and (b)) we observed an initial small enhancement of the low-temperature/high-field $H_{Irr}(T)$, followed by a drastic suppression. After the 600 and 700 °C HTs, the GB ILs reveal a particularly strong curvature, which is typically associated with Josephson weak-link behaviour. In contrast, the over-oxygenated samples (figures 3(c) and

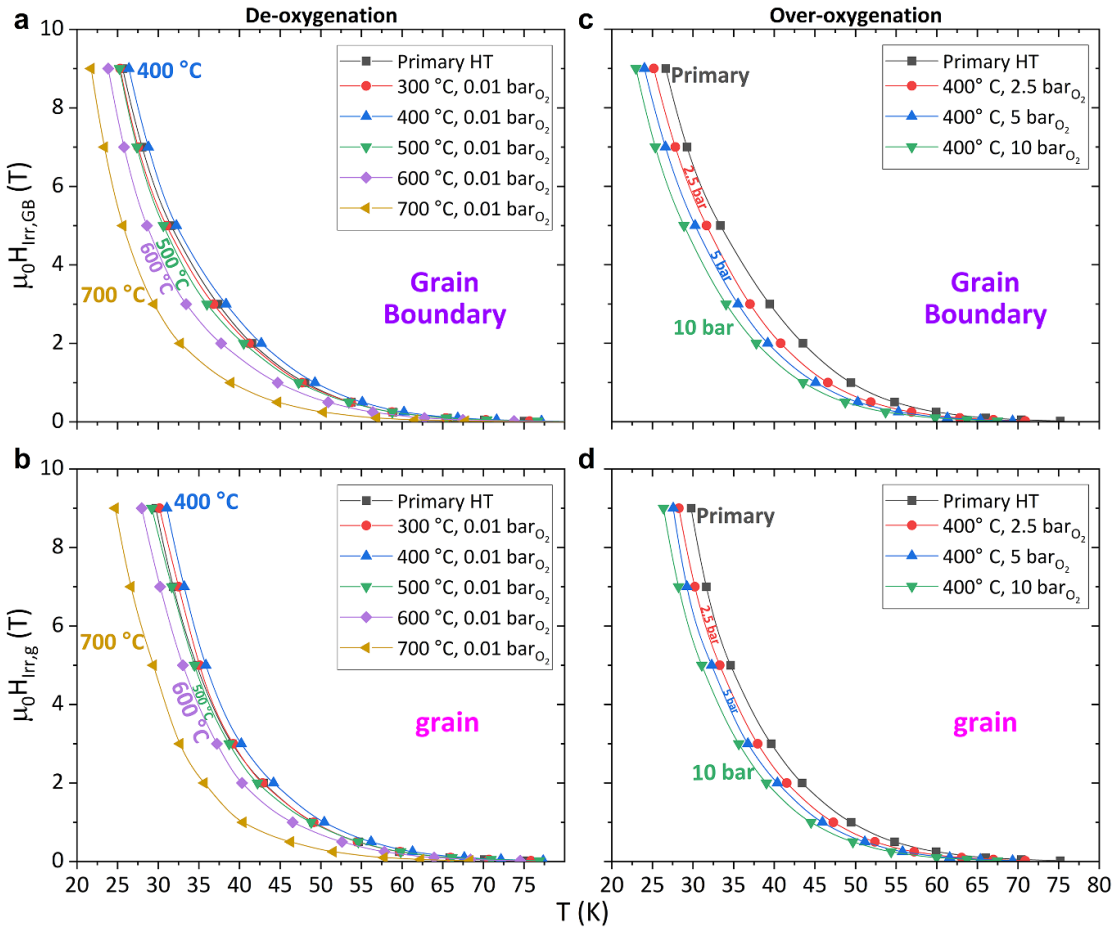


Figure 3. (a), (c) Grain boundary and (b), (d) grain irreversibility lines of $Bi_2Sr_2CaCu_2O_x$ samples at various doping states obtained by AC susceptibility. (a) and (b) are for the samples that underwent de-oxygenation and (c), (d) for the over-oxygenated samples. These curves show that after de-oxygenation the irreversibility lines move in temperature in a non-monotonic way, revealing also an increasing upward curvature with increasing the heat treatment temperature. In the over-oxygenation case, the irreversibility lines shift toward lower temperature but without significant change in the curve temperature dependence.

(d)) show $H_{\mathrm{Irr}}(T)$ curves that progressively shift toward lower temperatures with increasing oxygen level, although the overall shape of the curves remained relatively unchanged. In all samples the GB IL always lies below that of the grains.

To better understand the low-temperature trend of the ILs as a function of doping state, figure 4 presents the irreversibility temperatures $T_{\mathrm{Irr,GB}}$ and $T_{\mathrm{Irr,g}}$ evaluated at 9 T (the maximum applied DC field) for the GBs and grains, respectively, as a function of p_{GB} and p_{g}. We observed that the grain $T_{\mathrm{Irr,g}}\left(p_{\mathrm{g}}\right)$ (figure 4(b)) peaked at about $p_{\mathrm{g}} \sim 0.19$, corresponding to the sample de-oxygenated at 400 °C, with sharp declines on either side of this doping level. Within the studied doping range $T_{\mathrm{Irr,g}}$ varies by more than 6 K, from ∼24.7 K in the under-doped state ($p_{\mathrm{g}} \sim 0.146$) to the maximum of ∼31.1 K ($p_{\mathrm{g}} \sim 0.188$). On the other hand, the GB behaviour of $T_{\mathrm{Irr,GB}}\left(p_{\mathrm{GB}}\right)$ is less systematic (figure 4(a)), with $T_{\mathrm{Irr,GB}}$ showing less than 1.5 K variation in the $p_{\mathrm{GB}} \sim 0.153 - 0.196$ range, but decreasing rapidly outside this range, reaching an overall variation of almost 5 K. A peculiar feature of the $T_{\mathrm{Irr,GB}}\left(p_{\mathrm{GB}}\right)$ trend is the presence of two distinct maxima at $p_{\mathrm{GB}} \sim 0.16$ and 0.18.

To understand the origin of the different $T_{\mathrm{Irr,g}}\left(p_{\mathrm{g}}\right)$ and $T_{\mathrm{Irr,GB}}\left(p_{\mathrm{GB}}\right)$ trends, we need to consider both the measurement technique and the sample microstructure. Since they are obtained inductively via AC susceptibility, the long-range GB ILs reflect current percolation through both the well-connected GBs and the grains. Since along the wire the grains assume any and all *c*-axis orientations (Bi-2212 grains are locally biaxial textured, but along the wire the *c*-axis direction changes), the GB ILs are constrained by the least favourable grain orientations and the worst GBs with respect to the local field orientation. On the other hand, the short-range grain ILs are determined by intra-grain currents only. Since the grains assume any orientation with respect to the field, the grain ILs represent an average of ILs for all grain orientations. As shown in figure 4(b), the single sharp maximum of $T_{\mathrm{Irr,g}}\left(p_{\mathrm{g}}\right)$ at $p_{\mathrm{g}} \sim 0.19$ indicates that on average the best doping level for the grain IL is at the grain critical doping p_{c}, achieved by

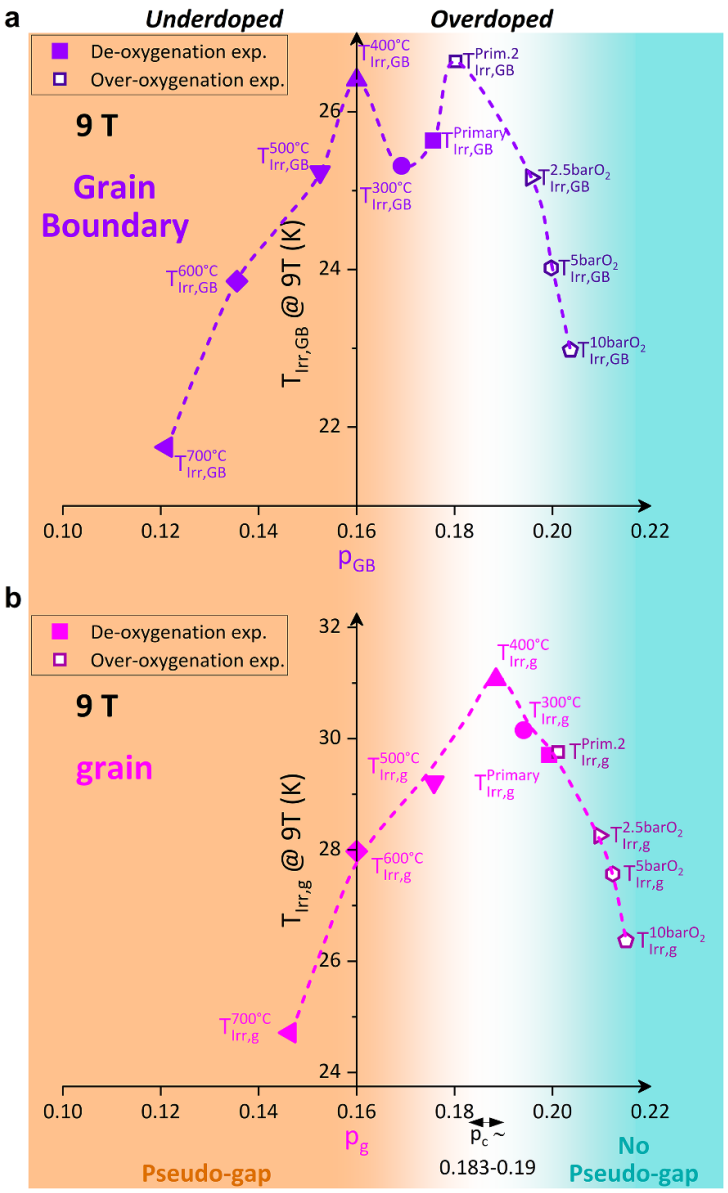


Figure 4. (a) Grain boundary and (b) grain irreversibility temperatures $T_{\mathrm{Irr,GB}}$ and $T_{\mathrm{Irr,g}}$ at 9 T as a function of doping concentrations in $Bi_2Sr_2CaCu_2O_x$ samples. The T_{Irr} values are from figure 3 and the p values are from figure 2. The grain boundary irreversibility temperature $T_{\mathrm{Irr,GB}}$ at 9 T as a function of the grain boundary doping p_{GB} shows a non-monotonic behaviour with two maxima in the samples with either the grain (400 °C de-oxygenation) or the grain boundaries (Prim.2) close to the critical doping p_c. The grain irreversibility temperature $T_{\mathrm{Irr,g}}$ at 9 T as a function of the grain doping p_g has a single maximum for the sample with the grain doping at p_c.

the 400 °C de-oxygenation. In contrast, the peculiar two-maxima feature of $T_{\mathrm{Irr,GB}}(p_{\mathrm{GB}})$ (figure 4(a)) can be explained by considering both p_{GB} and the specific samples where the maxima are observed: the maximum at $p_{\mathrm{GB}} \sim 0.18$ is indeed near the GB critical doping p_c, where the pseudo-gap is barely open, whereas the $p_{\mathrm{GB}} \sim 0.16$ maximum is in the sample de-oxygenated at 400 °C, with the grains at their critical doping. This implies that in this temperature range (∼22–26 K) the GB ILs are influenced by both the grain and the GBs pseudo-gaps and, since the grain and the GBs do not reach their respective p_c in the same sample, this results in the observed $T_{\mathrm{Irr,GB}}(p_{\mathrm{GB}})$ double feature.

3.3. Change of the critical current density with the doping state

Because Bi-2212 is intended for low-temperature applications, we performed the critical current density measurements at 4.2 K and 5 T on all samples to evaluate its dependence on the doping level. Transport J_c is inherently a long-range characterization involving both the grains and the GBs and, since J_c in HTS is typically limited by the GB properties, it might appear more logical to plot J_c as a function of p_{GB}. However, we chose to examine the trends with respect to both p_{GB} and p_g (figure 5). We observed that de-oxygenation at temperature up to 400 °C led to a marginal increase in J_c (up to 3%) compared to

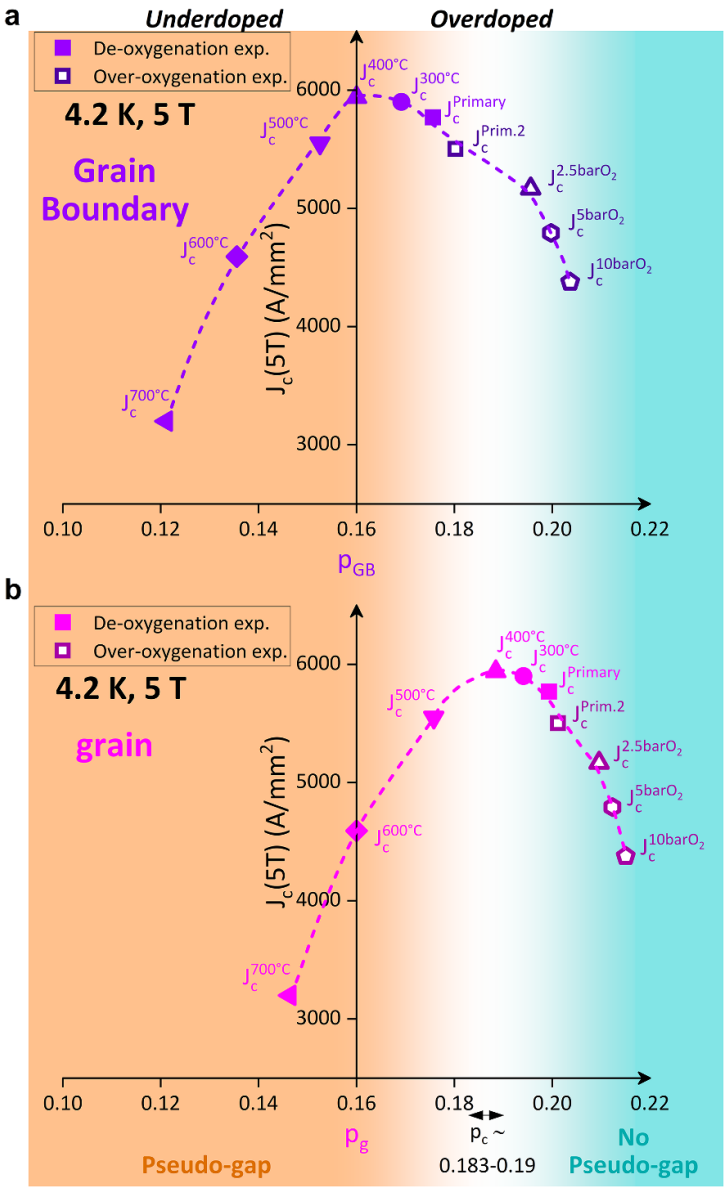


Figure 5. Transport critical current density J_c (5 T, 4.2 K) as a function of (a) the grain boundary and (b) the grain doping concentrations in $Bi_2Sr_2CaCu_2O_x$ samples. The p values are from figure 2. These doping concentration dependences reveal that the grain doping is more strongly affecting J_c leading to a maximum at the grain critical doping p_c.

the primary heat-treated sample. Further de-oxygenation resulted in a sharp J_c decrease and a systematic J_c suppression was also observed in the over-oxygenated samples. The 400 °C de-oxygenated sample with the maximum J_c corresponds at the same time to the optimal doping for the GBs (maximum $T_{c,GB}$ at $p_{GB} = 0.16$) and to the critical doping for the grains ($p_g \sim 0.19$).

The presence of a single maximum in $J_c\,(4.2\,\mathrm{K}, 5\,\mathrm{T})$, similar to $T_{\mathrm{Irr,g}}\left(p_g\right)$ (figure 4(b)), suggests that at low temperature the grain properties have a stronger influence on J_c than the GBs. However, $J_c\left(p_g\right)$ maximum is less sharp than that of $T_{\mathrm{Irr,g}}\left(p_g\right)$, and the J_c decline on the high-p side is more gradual. This indicates that transport J_c is also sustained by the relatively stable GB IL in these samples (see figures 4(a) and 5(a) in the $p_{GB} \sim 0.16 - 0.18$ range). Overall, these observations suggest that J_c is affected by both the grain and the GB doping levels, and specifically by the presence or absence of their respective pseudo-gaps.

4. Discussion

Performing secondary HT on Bi-2212 wires after the standard OPHT enabled us to estimate the actual p concentration following both the primary HT and the subsequent de-oxygenation/over-oxygenation

experiments. We established that, after the primary HT, both the grain and the GBs were indeed in a slight over-doped state. However, a noticeable difference exists between their doping levels: the grains were above p_c while the GBs remain below it. Moreover, varying the oxygen content with secondary HTs consistently resulted in different doping levels for grains and GBs, implying that they cannot be simultaneously optimized.

The different doping states also led to distinct superconducting properties. We examined in detailed the grain and GB ILs, as well as the overall J_c performance. Since those characterizations were performed in different temperature ranges (the former at intermediate and high temperatures, the latter at low temperature) it is important to recall previously identified differences [15, 16]. In fact, we had found that an additional intra-grain pinning mechanism, presumably induced by point defects, emerges at low temperature in Bi-2212 wires. This mechanism also influences the overall inter-grain performance, but only to a limited extent in the 20–30 K range where H_{Irr} is measured. On the contrary, there is a clear correlation between the enhanced intra-grain pinning and the increased J_c at 4.2 K, explaining some of the trend differences observed across temperature ranges.

Our present investigation of the doping dependence of Bi-2212 revealed that the superconducting properties exhibit peculiar features when either the grains or the GBs are at their respective critical doping, indicating correlations between the sudden property changes and the opening of the pseudo-gap. In retrospect, it is not surprising that $T_{Irr,g}\left(p_g\right)$ shows a single maximum at the grain critical doping (in the 400 °C de-oxygenated sample), where also H_{c2} is expected to be maximized [10]. On the contrary, $T_{Irr,GB}$, which reflects overall sample properties, is influenced by both grain and GB doping levels resulting in two maxima, one at the GB critical doping and the other where the grain doping is at p_c.

The critical current density, being measured at lower temperature and field, lies in a regime of strong superconductivity, considering that at 4.2 K H_{Irr} is also expected to approach H_{c2}. The maximum J_c value, obtained in the 400 °C de-oxygenated sample with $p_g \sim 0.19$, is only marginally better than that of the primary-heat-treated sample. This single J_c maximum aligns with our previous findings that $J_c\left(4.2\ \mathrm{K}\right)$ was affected by the intra-grain pinning properties. Unfortunately, because grain and GBs reach their critical doping in different samples, the secondary HTs produce only a modest $J_c\left(p_g\right)$ plateau, rather than a sharp peak. Previous study on Bi-2212 films revealed a sharp maximum at $p_c = 0.19$, with J_c dropping rapidly above p_c but more gradually below it (with a secondary broad trend peaking at $p = 0.16$) [19]. Interestingly, the ratio $J_c\left(p = 0.19\right)/J_c\left(p = 0.16\right)$ is about 2.2 in these films, whereas in our samples $J_c\left(p_g = 0.19\right)/J_c\left(p_g = 0.16\right)$ is less than 1.3, indicating some GB limitations. This suggests that if both grains and GBs could be simultaneously tuned to their critical doping levels, a significant increase in J_c, potentially over 60%, could be achieved.

Although J_c is affected by the intra-grain pinning, the GBs inevitably play an important role due to their involvement in the current percolation. Previous studies have shown that increasing filament bonding negative impacts J_c, as a result of associated microstructural changes [13, 14, 16]. In fact, extensive bonding degrades the Bi2212 texture, presumably leading to a broader biaxial grain orientation distribution. However, other factors may in general contribute. For instance, it has not yet been investigated whether the microchemical composition (other than oxygen content) is altered at GBs by varying heat-treatment parameters, and whether such changes might be significant enough to also affect the grain composition, so affecting the overall connectivity. In the present study, this is not expected to be a major factor, as the microstructure is predominantly established during the primary OPHT.

The pseudo-gap is a physical phenomenon of other HTSs, including REBCO. Although the nature of the GBs differs significantly between REBCO and Bi-2212 conductors (REBCO counts on *ab*-plane current percolation with low-angle GBs to avoid the exponential I_c decay beyond the critical angle in [001]-tilted GBs [20], whereas Bi-2212 most likely relies on *c*-axis percolation through GBs closer to [001]-twist configuration [21]), separate openings of the pseudo-gap may also occur in REBCO, potentially generating differences in the grain and GB properties. Consequently, optimizing GB properties in other HTS materials may further enhance their performance. This possibility warrants investigation, as it could lead to improvements of the state-of-the-art conductors with positive effects for applications, like magnets or cables.

5. Conclusion

The separate characterization of the grain and GB properties upon varying the doping, from the underdoped to the over-doped states and across the critical doping, was done here for the first time in Bi-2212 conductors. This work clearly demonstrated that the superconducting performance presents clear

features in correspondence of doping previously identified as critical, making us infer that Bi-2212 conductors are independently affected by the separate openings of the pseudo-gap in the grain and at GBs, leading to non-trivial trends for the IL behaviour. In contrast, the low-temperature J_c, which is more strongly influenced by intra-grain vortex pinning and less by the GB irreversibility field, exhibits a single broad maximum with changing doping, but less pronounced than the strong J_c peak observed in thin films [19]. It seems that attaining the ultimate performance of Bi-2212 wires would require separate tuning of the grains and GBs to their individual critical doping levels, which is, almost certainly, challenging. In fact, it would require designing HTs capable of setting grains and GBs to different doping levels. Because oxygen diffuses more readily into the GBs than into the grains, low-temperature, high-oxygen-pressure HTs could in principle modify GB doping more rapidly than grain doping. This could be pursued either by additional heat-treatment steps after the primary HT or by changing the final stages of the primary HT. However, the primary HT is already rather complex [14]. Moreover, while such tailored treatments might enhance the performance of state-of-the-art Bi-2212 wires in short lengths, achieving this level of doping control at magnet scales would be extremely difficult, suggesting that alternative approaches may ultimately be more beneficial. Other high-temperature superconductors might present a different situation. Although they also could suffer from GB limitations due to the different doping level and possible separate opening of the pseudo-gap with respect to the grains, they may be easier to process. These results clearly underscore the complexity of these fascinating materials.

Acknowledgments

This work is funded by the US Department of Energy, Office of Science, and Office of High Energy Physics under Award Number DE-SC0010421 and performed under the purview of the US-Magnet Development Program. This work was performed at the National High Magnetic Field Laboratory, which is supported by National Science Foundation Cooperative Agreements NSF DMR-2128556, and by the State of Florida. We are grateful to Jozef Kvitkovic of NHMFL for the measurement of critical current for the over-oxygenated samples.

Data availability statement

The data that support the findings of this study are openly available at the following URL/DOI: https://osf.io/7bd64/ [22].

Author contributions

Chiara Tarantini 0000-0002-3314-5906
Conceptualization (equal), Data curation (lead), Formal analysis (lead), Investigation (lead), Methodology (lead), Writing – original draft (lead)

Shaon Barua 0000-0001-7027-2077
Data curation (equal), Formal analysis (equal), Investigation (equal), Methodology (equal), Writing – review & editing (equal)

Jianyi Jiang 0000-0002-1094-2013
Data curation (equal), Formal analysis (equal), Funding acquisition (equal), Investigation (equal), Methodology (equal), Writing – review & editing (equal)

Fumitake Kametani 0000-0002-1067-9331
Conceptualization (equal), Funding acquisition (equal), Writing – review & editing (equal)

Eric E Hellstrom 0000-0001-8263-8662
Conceptualization (equal), Funding acquisition (equal), Methodology (equal), Writing – review & editing (equal)

David C Larbalestier 0000-0001-7098-7208
Conceptualization (equal), Funding acquisition (equal), Methodology (equal), Writing – review & editing (equal)

References

[1] Bardeen J, Cooper L N and Schrieffer J R 1957 Microscopic theory of superconductivity *Phys. Rev.* **106** 162–4
[2] Keimer B, Kivelson S A, Norman M R, Uchida S and Zaanen J 2015 From quantum matter to high-temperature superconductivity in copper oxides *Nature* **518** 179–86
[3] Presland M R, Tallon J L, Buckley R G, Liu R S and Flower N E 1991 General trends in oxygen stoichiometry effects on T_c in Bi and Tl superconductors *Physica C* **176** 95–105
[4] Tallon J L 1998 Normal-state pseudogap in $Bi_2Sr_2CaCu_2O_8$ characterized by impurity scattering *Phys. Rev. B* **58** R5956–9
[5] Loram J W, Luo J L, Cooper J R, Liang W Y and Tallon J L 2000 The condensation energy and pseudogap energy scale of Bi: 2212 from the electronic specific heat *Physica C* **341–348** 831–4
[6] Chen S-D *et al* 2019 Incoherent strange metal sharply bounded by a critical doping in Bi2212 *Science* **366** 1099–102
[7] Norman M R, Pines D and Kallin C 2005 The pseudogap: friend or foe of high T c ? *Adv. Phys.* **54** 715–33
[8] Kordyuk A A 2015 Pseudogap from ARPES experiment: three gaps in cuprates and topological superconductivity (Review article) *Low Temp. Phys.* **41** 319–41
[9] Tallon J L, Storey J G, Cooper J R and Loram J W 2020 Locating the pseudogap closing point in cuprate superconductors: absence of entrant or reentrant behavior *Phys. Rev. B* **101** 174512
[10] Kim G C, Cheon M, Kim H, Kim Y C and Jeong D Y 2005 Hole concentration dependence of penetration depth and upper critical field in $Bi_2Sr_2(Ca,Y)Cu_2O_{8+\delta}$ extracted from reversible magnetization *Phys. Rev. B* **72** 064525
[11] Tallon J L, Williams G V M and Loram J W 2000 Factors affecting the optimal design of high-T superconductors—the pseudogap and critical doping q *Physica C* **338** 9–17
[12] Larbalestier D C *et al* 2014 Isotropic round-wire multifilament cuprate superconductor for generation of magnetic fields above 30 T *Nat. Mater.* **13** 375–81
[13] Kametani F, Jiang J, Matras M, Abraimov D, Hellstrom E E and Larbalestier D C 2015 Comparison of growth texture in round Bi2212 and flat Bi2223 wires and its relation to high critical current density development *Sci. Rep.* **5** 8285
[14] Jiang J *et al* 2023 Performance and microstructure variation with maximum heat treatment temperature for recent Bi-2212 round wires *IEEE Trans. Appl. Supercond.* **33** 6400105
[15] Tarantini C, Oloye T A, Hossain S I, Kametani F, Jiang J, Hellstrom E E and Larbalestier D C 2023 ac susceptibility studies of intra- and intergrain properties of high-J_c Bi-2212 wires *Phys. Rev. Mater.* **7** 014802
[16] Tarantini C, Barua S, Oloye T A, Kametani F, Jiang J, Hellstrom E E and Larbalestier D C 2024 Variation of effective filament diameter, irreversibility field, anisotropy, and pinning efficiency in Bi-2212 round wires *Supercond. Sci. Technol.* **37** 015021
[17] Gömöry F and Takács S 1993 Irreversibility line and non-linearity in the AC response caused by flux pinning in high-Tc superconductors *Physica C* **217** 297–312
[18] Matras M R, Jiang J, Larbalestier D C and Hellstrom E E 2016 Understanding the densification process of $Bi_2Sr_2CaCu_2O_x$ round wires with overpressure processing and its effect on critical current density *Supercond. Sci. Technol.* **29** 105005
[19] Naamneh M, Campuzano J C and Kanigel A 2014 Doping dependence of the critical current in $Bi_2Sr_2CaCu_2O_{8+\delta}$ *Phys. Rev. B* **90** 224501
[20] Dimos D, Chaudhari P and Mannhart J 1990 Superconducting transport properties of grain boundaries in $YBa_2Cu_3O_7$ bicrystals *Phys. Rev. B* **41** 4038–49
[21] Zhu Y, Li Q, Tsay Y N, Suenaga M, Gu G D and Koshizuka N 1998 Structural origin of misorientation-independent superconducting behavior at [001] twist boundaries in $Bi_2Sr_2CaCu_2O_{8+\delta}$ *Phys. Rev. B* **57** 8601
[22] Tarantini C 2026 Effects of the pseudo-gap on the superconducting performance of $Bi_2Sr_2CaCu_2O_x$ round wires OSF repository (available at: https://osf.io/7bd64/)